INTERNATIONAL JOURNAL OF HYDROGEN ENERGY 42 (2017) 11980–11995

Available online at www.sciencedirect.com

ScienceDirect

journal homepage: www.elsevier.com/locate/he

Review Article

A coupled diffusion and cohesive zone modelling approach for numerically assessing hydrogen embrittlement of steel structures

L. Jemblie [a,*], V. Olden [b], O.M. Akselsen [a,b]

[a] Department of Engineering Design and Materials, NTNU, 7456 Trondheim, Norway
[b] SINTEF Materials and Chemistry, 7456 Trondheim, Norway

ARTICLE INFO

Article history:
Received 7 December 2016
Received in revised form
22 February 2017
Accepted 28 February 2017
Available online 23 March 2017

Keywords:
Hydrogen embrittlement
Hydrogen transport
Cohesive zone modelling
Finite element analysis
Fracture mechanics

ABSTRACT

Simulation of hydrogen embrittlement requires a coupled approach; on one side, the models describing hydrogen transport must account for local mechanical fields, while on the other side, the effect of hydrogen on the accelerated material damage must be implemented into the model describing crack initiation and growth. The present study presents a review of coupled diffusion and cohesive zone modelling as a method for numerically assessing hydrogen embrittlement of a steel structure. While the model is able to reproduce single experimental results by appropriate fitting of the cohesive parameters, there appears to be limitations in transferring these results to other hydrogen systems. Agreement may be improved by appropriately identifying the required input parameters for the particular system under study.

Contents

* Corresponding author.
E-mail address: lise.jemblie@ntnu.no (L. Jemblie).
http://dx.doi.org/10.1016/j.ijhydene.2017.02.211

Introduction

Hydrogen induced degradation of mechanical properties, often termed hydrogen embrittlement (HE), is a well recognized threat for structural steels. It manifests as loss in ductility, strength and toughness, which may result in unexpected and premature catastrophic failures. The phenomenon was first reported by Johnson in 1874 [1], and has later been extensively researched both experimentally [2–11] and numerically [12–20], yielding a number of models accounting for the phenomenon. However, no consensus about the basic mechanisms responsible for hydrogen embrittlement is reached yet. Two theories have advanced as the more accepted ones for the case of hydrogen degradation in steel: Hydrogen Enhanced Decohesion (HEDE), in which interstitial atomic hydrogen reduces the bond strength and thus the necessary energy to fracture [21–25]; and Hydrogen Enhanced Localized Plasticity (HELP), in which atomic hydrogen accelerates dislocation mobility through an elastic shielding effect which locally reduces the shear stress [26–30]. Today it is seemingly recognized that no single mechanism can comprehensively explain all the phenomena associated with hydrogen embrittlement. Rather it appears that different mechanisms apply to different systems, and that a combination of mechanisms is more likely in many cases.

In recent years, cohesive zone modelling has gained increasing interest as suitable method for modelling hydrogen embrittlement [14–16,18,20,31,32], with the possibility of providing increased understanding of the involved process and their interactions combined with reduced time and costs compared to experimental programs. The damage process is classically described by interface elements, which constitutive relation is defined by a cohesive law (traction separation law). Simulation of hydrogen induced degradation requires a coupled approach, including modelling of transient mass transport, plastic deformation, fracture and their interactions. On one side, the models describing hydrogen diffusion must account for local mechanical field quantities; i.e. hydrostatic stress and plastic strain. On the other side, the effect of hydrogen on the accelerated material damage must be implemented into the cohesive law.

The present work presents a review of coupled diffusion and cohesive zone modelling as a method for numerically assessing the hydrogen embrittlement susceptibility of a steel structure. In the first section, established and recent models for hydrogen transport are summarised and discussed. The second section gives an overview of cohesive zone modelling in general and approaches for implementing hydrogen influence. The coupling aspect between hydrogen transport and cohesive zone modelling is discussed and put in conjunction with the presented hydrogen diffusion models. Finally, in the third section, some practical applications of the presented model are discussed.

Hydrogen transport models

The process that results in hydrogen embrittlement includes a transport stage of hydrogen to the site of degradation. In order to predict the degrading effect of hydrogen on the mechanical properties, it is of fundamental importance to correctly assess the hydrogen distribution in the material.

Atomic hydrogen is generally considered to reside either at normal interstitial lattice sites (NILS) or being trapped at microstructural defects like dislocations, carbides, grain boundaries and interfaces. Traps generally reduce the amount of mobile hydrogen, thus decreasing the apparent diffusivity and increasing the local solubility of the system. To date, models of transient hydrogen diffusion generally account for trapping by dislocations and hydrostatic drift. Recent approaches include capturing the effect of geometrically necessary dislocations, multiple trap sites and hydrogen transport by dislocations [17,33–35].

Hydrogen in lattice

Given a metal lattice, the hydrogen concentration in NILS, C_L, can be expressed by [12]

$$C_L = \beta \theta_L N_L \tag{1}$$

with θ_L being the lattice site occupancy, N_L the density of solvent atoms and β the number of NILS per solvent atom, usually assigned to be 6 under the assumption of tetrahedral site occupancy in bcc iron. The density of solvent atoms, N_L, can be calculated through

$$N_L = \frac{N_A}{V_M} \tag{2}$$

where N_A is the Avogadro constant equal to $6.022 \cdot 10^{23}$ mol^{-1}, and V_M is the molar volume of the host lattice, which for iron is $7.106 \cdot 10^{-6}$ m^3/mol at room temperature. According to Equation (1), this gives a lattice occupancy to NILS concentration ratio of $\theta_L / C_L = 10^{-5}$ wppm^{-1}, and thus $\theta_L \ll 1$ for most practical purposes.

Hydrogen in traps

Similarly as for lattice sites, the hydrogen concentration in a specific trapping site, C_T, can be expressed by [12]

$$C_T = \alpha \theta_T N_T \tag{3}$$

where θ_T is the occupancy, N_T is the density of the specific trap site (dislocation, carbide etc.) and α is the number of sites per trap.

The ability of a trap site to hold hydrogen is associated with the trap binding energy, representing the attractive interaction of a trap site compared to a normal lattice site. Trap sites and trap binding energies can be established experimentally for a microstructure using varies approaches like electrochemical permeation or thermal desorption spectroscopy (TDS), with TDS considered best suited to provide detailed trap characteristics [5,17,36]. A considerable amount of data is reported in literature for various steels. Selected data on trap binding energies are summarized in Table 1, where the large discrepancy in binding energies for similar trapping sites reflects variations in microstructural features and experimental details.

Traps with a binding energy above 60–70 kJ/mol are typically denoted irreversible traps [43], characterized by a high binding energy not possible to overcome by normal tempering procedures. These hydrogen atoms may be regarded as permanently removed from the diffusion process.

There have been significant advances in theoretical approaches to capture the effect of traps on hydrogen transport, with models by McNabb and Foster [44] and Oriani [22] describing the process for steel. Oriani [22] proposed that hydrogen in NILS and hydrogen in reversible traps are always in local equilibrium, an approach which is valid in the domain of rapid trap filling and escape kinetics, such that

$$\frac{\theta_T}{1-\theta_T} = \frac{\theta_L}{1-\theta_L}\exp\left(\frac{E_B}{RT}\right) \tag{4}$$

with E_B being the trap binding energy. Considering that $\theta_L \ll 1$ for most purposes, C_L and C_T relates through

$$C_T = \frac{K\frac{\alpha N_T}{\beta N_L}C_L}{1+\frac{K}{\beta N_L}C_L} \tag{5}$$

where K is the equilibrium constant, as defined by the exponential term in Equation (4). A consequence of this equilibrium assumption is that the trap site occupancy becomes independent of the number of traps. By making use of Equations (1), (2) and (4), contours of the trap binding energy as a function of the trap occupancy and the NILS concentration are plotted in Fig. 1. The theoretical solubility of hydrogen in steel at normal temperature and pressure, measured in wppm, is on the order of 10^{-4} for α-iron [40] and 1 for austenitic stainless steels [45]. It is noticeable that for binding energies greater than about 60 kJ/mol, all traps will be completely saturated, $\theta_T \approx 1$ (unless C_L is small, less than 10^{-4} wppm). In contrast, traps with binding energies below 10–15 kJ/mol will be drained of hydrogen, $\theta_T \approx 0$ (unless C_L has a high value in excess of 10 wppm).

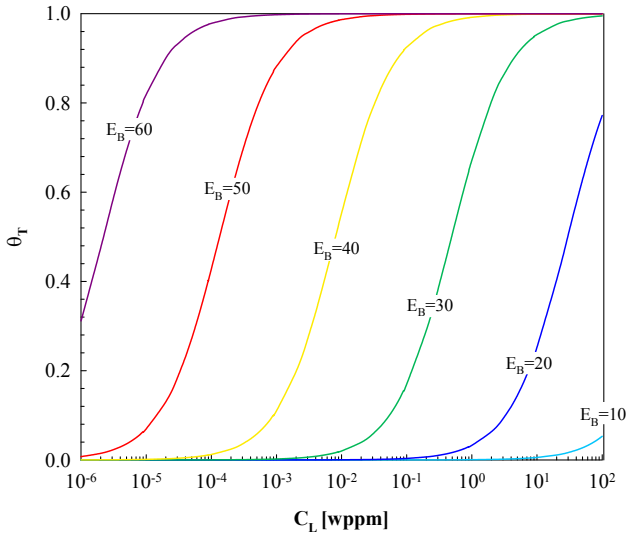

Fig. 1 – Relationship between NILS concentration, trap occupancy and trap binding energy, as proposed by Oriani [22]. The binding energy E_B is given in units of kJ/mol.

Table 1 – Selected trap binding energies for hydrogen in steel.

Trap site	E_b [kJ/mol]	Steel	Ref.
Dislocation	24–26.8	Ferritic	[3,37]
	10–20	Austenitic	[38,39]
Elastic dislocation	0–20.2	–	[17,40]
Screw dislocation core	20–30	–	[40]
Mixed dislocation core	59.9–61	–	[2,5]
Grain boundary	17.2–59	–	[3,17,37,40,41]
Austenite-ferrite interface	52	Duplex	[42]
Carbide interface	67–94	–	[5,17,37,40,41]

For microstructural defects like carbides and grain boundaries, the trap densities are often assumed constant throughout the material. For dislocations, however, the trap density varies point-wise dependent on the local plastic strain. Kumnick and Johnson [2] have studied hydrogen trapping in zone refined deformed iron by performing permeation transient measurements. By rolling at room temperature, 0–80% cold work were obtained. The resulting trap binding energies and trap densities were inferred from time lag measurements and interpreted in terms of the McNabb-Foster [44] approach. The trap density was found to increase sharply with deformation at low levels and more gradually with further deformation. Based on these observations, Sofronis and McMeeking [12] proposed the following relationship between the dislocation trap density, $N_T^{(d)}$, and the equivalent plastic strain, ε_p, for iron:

$$\log N_T^{(d)} = 23.26 - 2.33\exp(-5.5\varepsilon_p) \tag{6}$$

Similar relationships can be determined experimentally for the applicable steel by performing hydrogen permeation measurements at various levels of plastic deformation.

An alternative approach has been proposed by Sofronis et al. [27,46], assuming one trap site per atomic plane threaded by a dislocation, maintaining that this is consistent with the experimental work of Thomas [38]. The dislocation trap density is then expressed as a function of the dislocation density ρ and the lattice parameter a

$$N_T^{(d)} = \sqrt{2}\,\frac{\rho}{a} \tag{7}$$

The dislocation density (measured in dislocation line length per cubic meter) is considered to vary linearly with the equivalent plastic strain according to

$$\rho = \begin{cases} \rho_0 + \gamma\varepsilon_p & \text{for } \varepsilon_p < 0.5 \\ 10^{16} & \text{for } \varepsilon_p \geq 0.5 \end{cases} \quad (8)$$

where $\rho_0 = 10^{10}$ line length/m^3, denotes the dislocation density at zero plastic strain, and $\gamma = 2.0 \cdot 10^{16}$ line length/m^3. Using the lattice parameter of bcc iron $a = 2.86$ Å, the trap densities according to the data from Kumnick and Johnson [2] and the model by Sofronis et al. [27,46] are compared in Fig. 2. It can be concluded that the model by Sofronis et al. yields a dislocation trap density about three orders of magnitude larger than the data by Kumnick and Johnson. The maximum trapped concentration as predicted by the Sofronis model is in line with measured hydrogen concentrations in ferritic steel (1.5–2.5 wppm [47]), while the data from Kumnick and Johnson is more comparable to the theoretical equilibrium solubility of hydrogen in iron.

Using Equations (1)–(5), the dislocation trapped hydrogen concentration, C_T, is calculated as a function of the lattice hydrogen concentration, C_L, in terms of the trapping models by Kumnick and Johnson [2] and Sofronis et al. [27,46], assuming $V_M = 7.106 \cdot 10^{-6}$ m^3/mol, $\beta = 6$, $\alpha = 1$ and room temperature. The results are displayed in Fig. 3 for two levels of equivalent plastic strain, 0 and 0.8, and three levels of trap binding energy, 20, 40 and 60 kJ/mol.

Generally, the trapped concentration increases with increasing lattice concentration and increasing trap binding energy, until saturation is reached. With a higher lattice concentration, more hydrogen is available for trapping. With a higher binding energy, the attractive interaction of the trap site increases and, correspondingly, more hydrogen atoms will reside in traps. This is consistent with Fig. 1, resulting in an increased trap occupancy level. A higher level of plastic strain increases the trap density and, thus, the overall trapped concentration of the system. The trap occupancy is maintained, which by definition is independent of the trap site density.

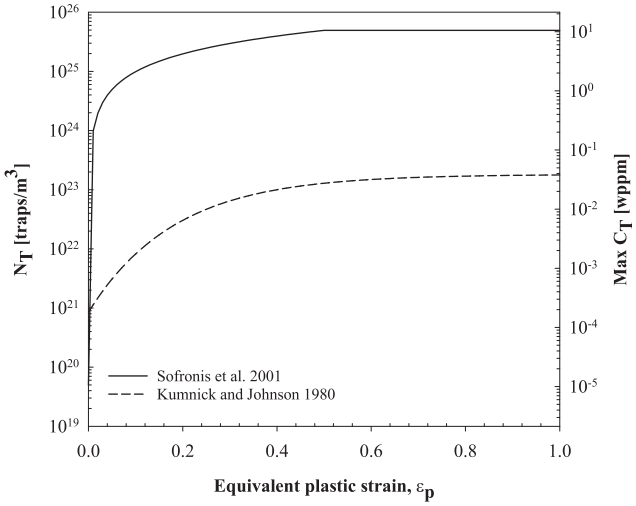

Fig. 2 – Dislocation trap densities according to the work by Kumnick and Johnson [2] and the model by Sofronis et al. [27,46]. In calculating C_T, it is assumed $\alpha\theta_T = 1$, which accordingly gives the maximum possible hydrogen concentration trapped at dislocations.

For $E_B = 60$ kJ/mol, all traps are saturated, and the trapped concentration is independent of the lattice concentration. Novak et al. [17] found that high-binding energy traps cannot account for the loss in strength observed on hydrogen charged steel, because these traps remain saturated with hydrogen regardless of loading conditions and/or hydrogen exposure conditions. Similar findings have been reported by Ayas et al. [48]. Rather, it is the lattice sites and low-binding energy trap sites which holds a critical role. Novak et al. [17] postulated that low-binding energy dislocation traps are the governing contribution promoting hydrogen induced fracture. On the other hand, Ayas et al. [48] reported that the presence of lattice hydrogen is the critical event with low energy trapped hydrogen only having a negligible effect.

It is noticeable from Fig. 3, that in most cases, either C_L or C_T yield the dominating influence on the total hydrogen concentration. Considering now only trapped concentration levels below saturation, $\theta_T \leq 1$. According to the trapping model by Kumnick and Johnson [2], assuming $\varepsilon_p \geq 0.8$ (maximum), trapping yields the dominating influence when $E_B \geq 37$ kJ/mol. Similarly, according to the model by Sofronis et al. [27,46], trapping yields the dominating influence when $E_B \geq 23$ kJ/mol. Conforming to the findings from Novak et al. [17] and Ayas et al. [48], assuming the only possible trap sites associated with hydrogen induced fracture are low-binding energy dislocations, it can be concluded that C_L will be the dominating influence on the total hydrogen concentration for most practical purposes.

Hydrogen diffusion

The main mechanism for hydrogen diffusion in steel is lattice diffusion by interstitial jumps, where the hydrogen atom occupy interstitial sites and move by jumping from one interstitial site to a neighbouring one [49].

Chemical potential gradients constitute the main driving force for hydrogen diffusion in steel; hydrogen will diffuse from regions where the chemical potential is high to regions where it is low, and the process ceases once the chemical potentials of all atoms are everywhere the same and the system is in equilibrium [50]. Assuming that the diffusion flux is proportional to the concentration gradient, which often is the case, Fick's laws are the governing equations describing the processes. These laws represent a continuum description and are purely phenomenological. Fick's first law gives the flux of diffusing particles, which for an isotropic medium is given by [51]

$$J = -D\frac{\partial C_L}{\partial x} \quad (9)$$

whit D being the lattice diffusion coefficient. The transient diffusion process is described by Fick's second law, also denoted the fundamental differential equation for diffusion [51]:

$$\frac{\partial C_L}{\partial t} = D\left(\frac{\partial^2 C_L}{\partial x^2} + \frac{\partial^2 C_L}{\partial y^2} + \frac{\partial^2 C_L}{\partial z^2}\right) \quad (10)$$

It can be derived from Equation (9) by considering a controlled volume element. The diffusion coefficient holds an Arrhenius-type dependence on temperature [45], such that

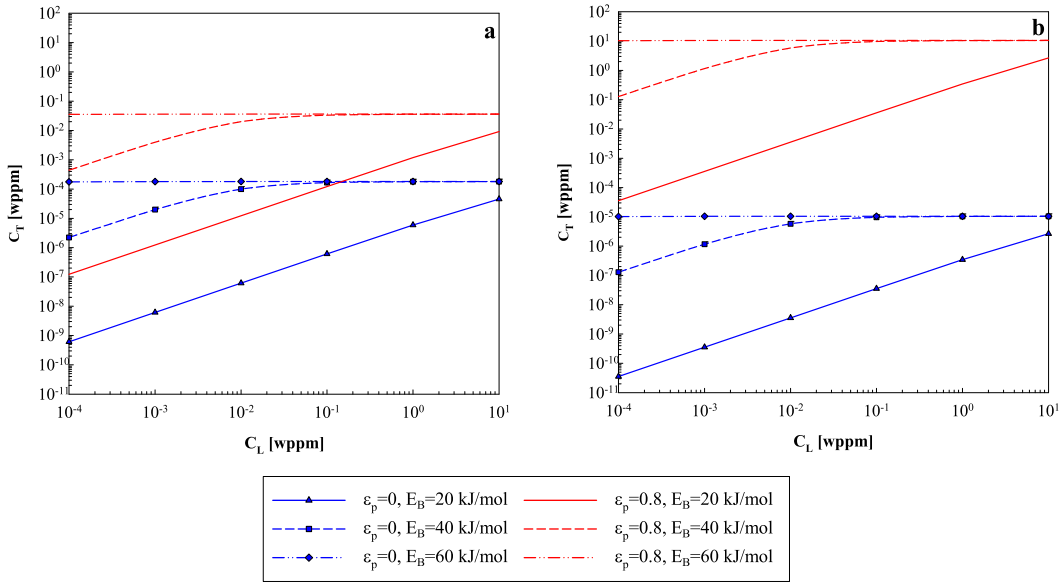

Fig. 3 – Plot of the trapped hydrogen concentration (C_T) as a function of the lattice hydrogen concentration (C_L), equivalent plastic strain (ε_p) and trap binding energy (E_B). (a) Trapping model by Kumnick and Johnson [2]. (b) Trapping model by Sofronis et al. [27,46].

$$D = D_0 \exp\left(\frac{-E_a}{RT}\right) \tag{11}$$

where D_0 is a pre-exponential factor independent of temperature and E_a is the activation energy (energy barrier) for hydrogen jumping between interstitial sites. Fig. 4 displays a summary of reported diffusion coefficients for hydrogen in iron and steel. The substantially higher diffusivity in ferrite compared to austenite is due to the lower packing density of bcc metals, reducing the potential energy barrier for jumps. In contrast, the larger interstice of fcc metals yields a higher hydrogen solubility in austenite. The large scatter observed for ferritic steels is generally considered to be associated with trapping [52].

Despite its small size, dissolved hydrogen atoms induces a distortion in the steel lattice, resulting in the formation of hydrostatic compressive stresses [53,54]. Any externally generated hydrostatic stress gradients in the system will therefore affect the resulting hydrogen diffusion and distribution. In terms of the chemical potential, Li et al. [55] have shown that it decreases with tensile stresses and increases with compressive ones. For a system under external stress, Fick's first law does therefore not sufficiently describe the diffusion flux. Rather, it is a function of both the concentration gradient and the gradient of hydrostatic pressure p, as given by

$$\mathbf{J} = -D\left(\nabla C_L + \frac{C_L \overline{V}_H}{RT}\nabla p\right) \tag{12}$$

where $\overline{V}_H$ is the partial molar volume of hydrogen, representing the unconstrained volume dilatation of the lattice containing one mole of hydrogen. Conforming to the requirement of mass conservation:

$$\frac{\partial}{\partial t}(C_L + C_T) = -\nabla \mathbf{J} \tag{13}$$

Sofronis and McMeeking [12] have derived an enhanced hydrogen transport model accounting for both trapping and hydrostatic drift:

$$\frac{\partial C_L}{\partial t} + \frac{\partial C_T}{\partial t} = \nabla(D\nabla C_L) + \nabla\left(\frac{D\overline{V}_H}{RT} C_L \nabla p\right) \tag{14}$$

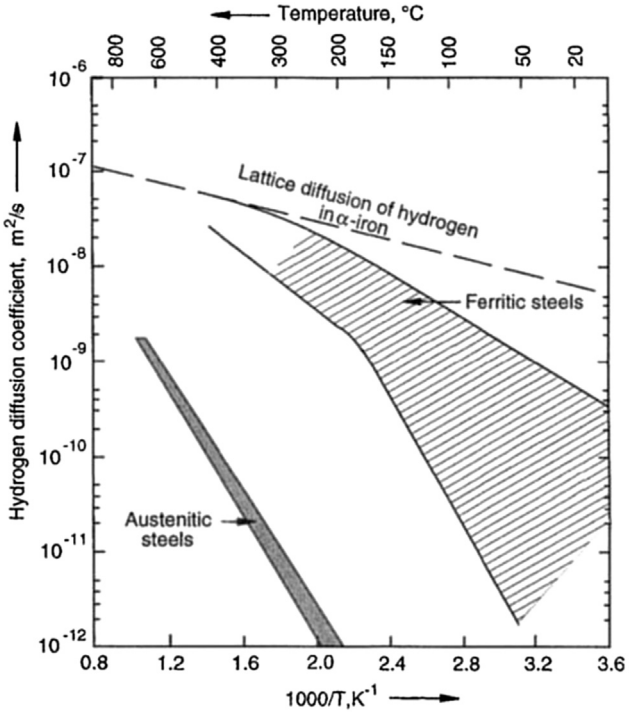

Fig. 4 – Reported diffusion coefficients for hydrogen in iron and steel. Adapted from Grong [52].

where C_T can be obtained following Oriani's equilibrium theory (Equation (4)). This model has been subsequently modified by Krom et al. [13], accounting for the effect of the strain rate on the transient hydrogen concentrations, finally giving:

$$\frac{C_L + C_T(1-\theta_T)}{C_L}\frac{\partial C_L}{\partial t} = \nabla(D\nabla C_L) + \nabla\left(\frac{D\overline{V}_H}{RT}C_L\nabla p\right) - \alpha\theta_T\frac{dN_T}{d\varepsilon_p}\frac{d\varepsilon_p}{dt} \tag{15}$$

The last term in this equation is the plastic strain rate factor, which disappears in the absence of dislocation trap sites ($dN_T/d\varepsilon_p = 0$). A first attempt in the direction of accounting for multiple trap sites has been made by Dadfarnia et al. [33], using an extension of Equation (15) and summing the contributions from each individual trap.

Implications of the hydrogen transport model

In the following section, the effect of varying the hydrogen solubility, the trap binding energy and the trap density on the total hydrogen distribution, as controlled by the hydrogen transport model in Equation (14), is illustrated. The boundary layer approach of small scale yielding under mode I opening is applied for a rounded notch with radius $R = 0.15$ mm. Displacements are enforced on the circular boundary, controlled by the stress intensity factor K_I. All input parameters and boundary conditions are given in Table 2, representative of a ferritic steel. The loading rate is chosen low enough to ensure adequate diffusion of hydrogen in a ferritic material, resembling a typical experimental set up for fracture mechanical testing of hydrogen embrittlement, maintaining a hydrogen lattice concentration close to steady state. The significant effect of strain rate on the lattice concentrations has previously been demonstrated by Krom et al. [13], and is as such not included in the present work.

Two trap density formulations are considered; the model by Kumnick and Johnson [2] in Equation (6), denoted the low trap density model, and a modified model given by

$$\log N_T^{(d)} = 25.75 - 2.33\exp(-5.5\varepsilon_p) \tag{16}$$

Table 2 – Input parameters and boundary conditions for FE hydrogen diffusion analysis.

Property	Symbol	Value
Young's modulus [MPa]	E	208,000
Poisson's ratio	ν	0.3
Yield strength [MPa]	$R_{p0.2}$	503
Tensile strength [MPa]	R_m	605
Diffusion coefficient [mm^2/s]	D	$1.19\cdot10^{-2}$ [40]
Initial bulk H concentration [wppm]	C_{L0}	0.00034, 1
Surface H concentration [wppm]	C_0	0.00034, 1
Trap binding energy [kJ/mol]	E_B	10–60
Molar volume of host lattice [mm^3/mol]	V_M	$7.11\cdot10^3$
Partial molar volume of H [mm^3/mol]	$\overline{V}_H$	$2\cdot10^3$ [40]
Number of NILS per host atom	β	6
Number of sites per trap	α	1
Temperature [°C]	T	20
Gas constant [J/K mol]	R	8.314
Stress intensity factor [MPa m$^{1/2}$]	K_I	200
Stress intensity factor rate [MPa m$^{1/2}$/s]	$\dot{K}_I$	$6.7\cdot10^{-4}$

where a larger initial trap density at zero plastic strain is assumed, denoted the high trap density model. The resulting hydrostatic stress and corresponding equivalent plastic strain at the end of loading is displayed in Fig. 5, reaching a maximum hydrostatic stress level of 1236 MPa 0.7 mm from the notch tip and a maximum equivalent plastic strain level of 0.624 at the notch tip.

Fig. 6a–d displays the resulting hydrogen profiles in front of the notch tip at the end of loading, for trap binding energies in the range 20–60 kJ/mol and two initial hydrogen concentrations of 0.00034 wppm and 1 wppm, representative of the theoretical solubility of hydrogen in ferrite and a 3% NaCl aqueous solution [15], respectively.

The effect of traps on the apparent diffusivity can be calculated by [22]

$$\frac{D_{\text{eff}}}{D} = \frac{C_L}{C_L + C_T(1-\theta_T)} \tag{17}$$

where D_{eff} is the effective diffusion coefficient. Assuming $E_B = 60$ kJ/mol, the effective diffusivity ratio at the notch tip yield 0.62 and 0.005 for the low and high trap density models, respectively, at an initial concentration of 0.00034 wppm. For an initial concentration of 1 wppm, the effective diffusivity ratio yield 1.0 and 0.94, respectively. Due to Oriani's equilibrium, increasing the lattice concentration also increases the trap occupancy (see Fig. 1), under the assumption of constant trap binding energy. In the limit of $\theta_T \to 1$, $D_{\text{eff}}/D = 1$, i.e. the traps yield no effect on the diffusion. Thus, when the lattice concentration is increased from 0.00034 wppm to 1 wppm, maintaining a constant trap binding energy level, the effective diffusivity will increase. The simulation results revealed only a negligible effect of trap binding energy and trap density on the lattice concentration, as most of the diffusion occurs ahead of the crack tip where the plastic strain level is lowered. In the plots, C_L is therefore included as one single line, representing all the cases considered.

The resulting trapped concentrations correspond well with the calculations in Figs. 1 and 3, reaching saturation at $E_B = 60$ kJ/mol and 40 kJ/mol for $C_0 = 0.00034$ wppm and 1

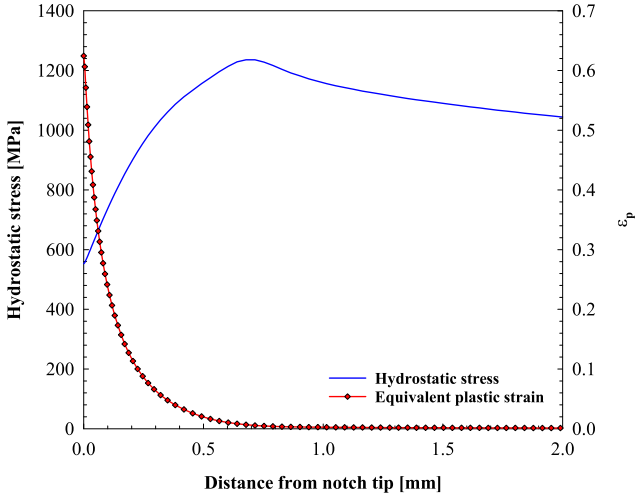

Fig. 5 – Hydrostatic stress and equivalent plastic strain as a function of the distance from the notch tip, plotted at the end of loading.

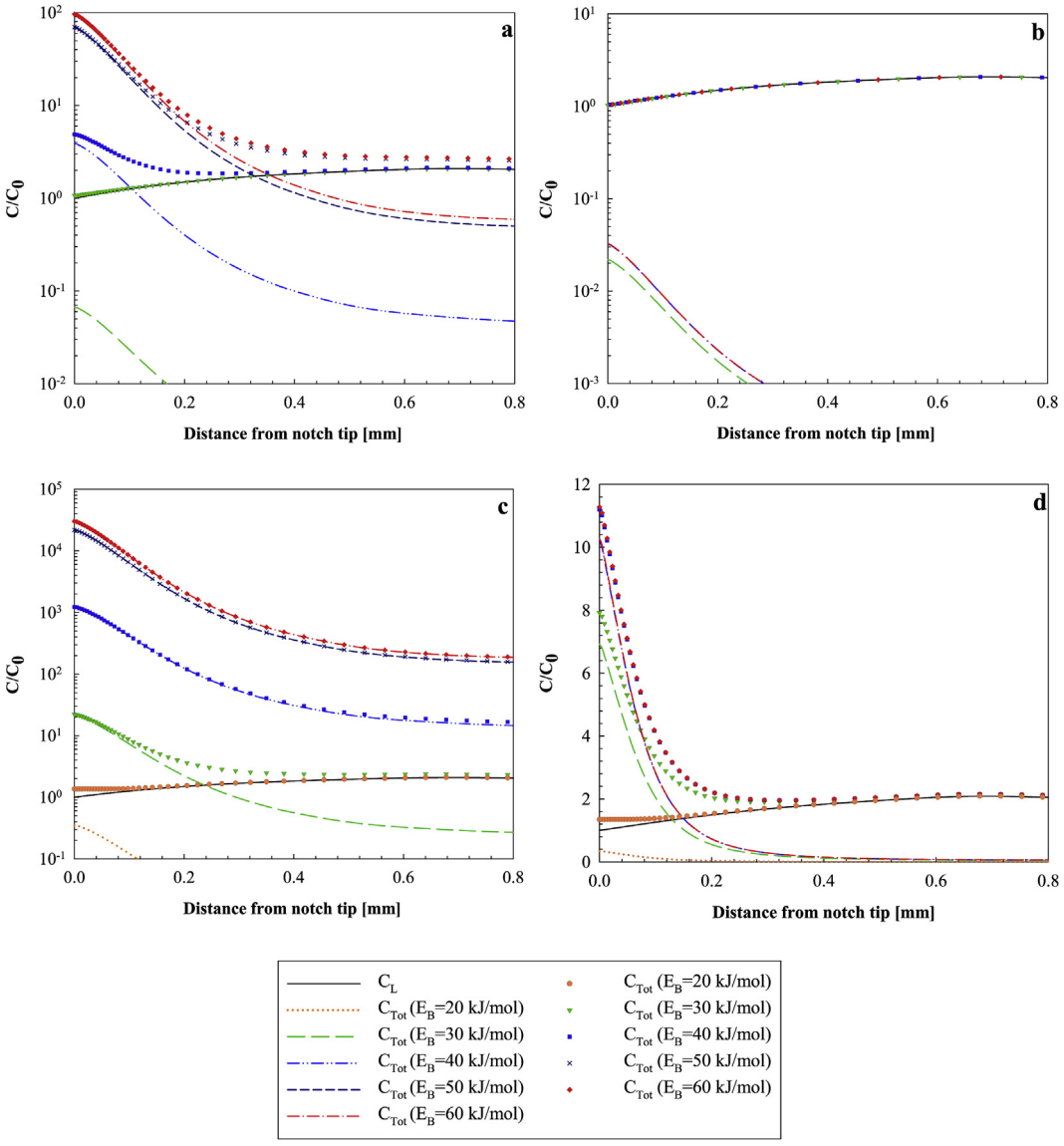

Fig. 6 – Normalized hydrogen concentration as a function of distance from the notch tip using the boundary layer approach, plotted at the end of loading. (a) Low trap density model, $C_0 = 0.00034$ wppm, $E_B = 30–60$ kJ/mol. (b) Low trap density model, $C_0 = 1$ wppm, $E_B = 30–40$, 60 kJ/mol. (c) High trap density model, $C_0 = 0.00034$ wppm, $E_B = 20–60$ kJ/mol. (d) High trap density model, $C_0 = 1$ wppm, $E_B = 20–40$, 60 kJ/mol.

wppm, respectively, independent of the trap density. For the low trap density model, the maximum attainable trapped concentration is 0.033 wppm, 100 times an initial lattice concentration of 0.00034 wppm. This concentration level is obtained for $E_B \geq 60$ kJ/mol. However for all $E_B \geq 40$ kJ/mol, the trapped concentration plays a significant role on determining the total concentration. With an initial concentration of 1 wppm, the trapped concentration plays no role on determining the total concentration, being at least 30 times lower than the lattice concentration.

For the high trap density model, the maximum attainable trapped concentration is 10.1 wppm, 30,000 times an initial lattice concentration of 0.00034 wppm. While this concentration level is only obtained for $E_B \geq 60$ kJ/mol, the trapped concentration plays a significant role on determining the total concentration for all designated binding energy levels. For all $E_B \geq 40$, it is the dominating factor. With an initial concentration of 1 wppm, the influence of the lattice concentration becomes more apparent, while the trapped concentration still plays a significant role on determining the total concentration close to the notch tip. Comparing the plots, trapping appears to hold the dominating influence on the total hydrogen concentration for all trap binding energy levels above 30 kJ/mol, except for the combination of high hydrogen solubility and low trap density in Fig. 6b. All this is true for the given C_L level in question.

A cohesive zone modelling approach to hydrogen embrittlement

Cohesive models were first formulated by Barenblatt [56] and Dugdale [57], who introduced finite non-linear cohesive tractions in front of an existing crack, as a mean to overcome the crack tip stress singularity. To date, the cohesive model is extensively applied for crack propagation analysis using the finite element method. Among the various approaches available, it is appealing in that it requires few parameters and in its universality of applicability [58].

The cohesive model

The cohesive theory of fracture is a purely phenomenological continuum framework, not representative of any physical material. The constitutive response of the material is divided in two parts; an arbitrary material law relating the stresses and strains in the bulk regions adjacent to the crack faces, and a cohesive law characterizing the separation process by describing the forces opposing crack formation (tractions) as a function of the incipient crack surfaces' separation distance. Common to most cohesive laws is that they can be described by two independent parameters out of the following three: the cohesive strength σ_C, the critical separation δ_C and the cohesive energy Γ_C. Fig. 7 displays three commonly applied cohesive laws, plotted as normalized traction versus separation; a linear decreasing law suggested for brittle materials by Hillerborg et al. [59], a polynomial law suggested by Needleman [60] for ductile materials and, more recently, a versatile trapezoidal law suggested by Scheider [61] also for ductile materials. The area embedded by the curve represents the cohesive energy. A more thorough compilation of cohesive laws can be found in literature, e.g. Shet and Chandra [62] or Brocks et al. [63].

An intrinsic disconnection exists between atomistic and engineering cohesive descriptions, where the fundamental formulation by Barenblatt [56] is equivalent to the atomistic conception of the cohesive zone. Typically, the work of separation differs by orders of magnitude, suggesting the engineering description contains elements of the plastic work of fracture. In cohesive zone modelling, the cohesive energy can physically be understood as the total energy dissipated by the cohesive element during separation.

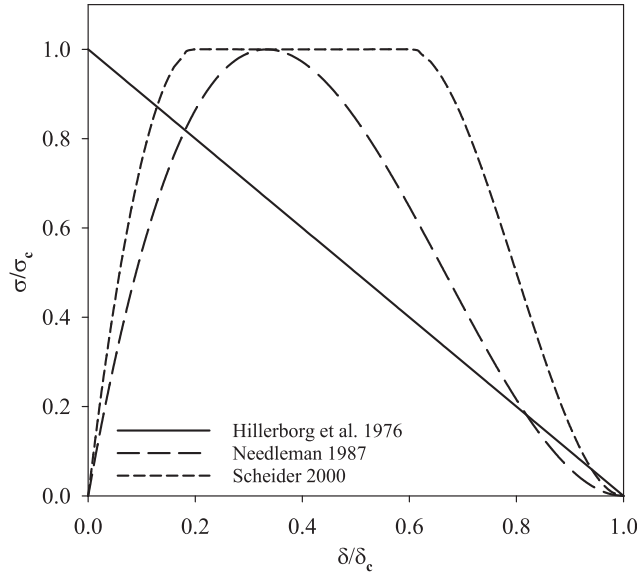

Fig. 7 – Cohesive laws by Hillerborg et al. [59], Needleman [60] and Scheider [61].

The influence of the shape of the cohesive law on the results is controversial; while Scheider and Brocks [64] found significant effect on their calculated results, Tvergaard and Hutchinson [65] concluded that such an influence is negligible. Irrespectively, the cohesive law has to be chosen in relation to the actual micromechanical damage mechanism leading to failure. Values of the cohesive parameters should be chosen so that they do not affect the overall compliance of the system [19]. Alvaro et al. [19] points out the importance of this in relation to modelling hydrogen embrittlement. A choice of cohesive parameters which infers low values of the initial stiffness will results in lower values of hydrostatic stress and equivalent plastic strain, consequently affecting the lattice and trapped hydrogen populations.

Despite cohesive zone simulation being straightforward, it has limitations when it comes to modelling crack nucleation, failing to produce a converged solution at the point were the crack first nucleates. These problems, which are especially prominent in performing a coupled hydrogen transport and cohesive analysis, are attributed to a snap-back instability that occurs just after the stress reaches the peak strength of the interface [66]. Gao and Bower [66] found that adding a small viscosity term in the cohesive relation significantly increases the numerical stability. Yu et al. [67] have applied the viscosity term by Gao and Bower [66] in a three step, uncoupled, hydrogen informed cohesive zone model under constant displacement, and found the viscous regularization to be effective in solving the convergence problem with good accuracy. In relation to performing a coupled hydrogen transport and cohesive analysis, it is still some uncertainty in whether a model containing this viscosity term is able to accurately predict the time to fracture.

Implementing hydrogen influence

Most known attempts of implementing hydrogen influence into the cohesive model is through the HEDE principle [15,19,20,68–70]; hydrogen reduction of the cohesive energy at fracture. In its most simplistic approach, the critical hydrogen dependent cohesive stress $\sigma_C(C)$ is assumed to decrease linearly with increasing hydrogen concentration

$$\sigma_C(C) = \sigma_C(0)(1 - \xi C) \tag{18}$$

where $\sigma_C(0)$ is the critical cohesive stress with no hydrogen influence and ξ is a softening parameter, often found by fitting to experimental results [70–72]. At the extreme, this formulation predicts a hydrogen influenced fracture toughness $K_{IC} = 0$ and, thus, complete decohesion upon the attainment of a certain critical hydrogen concentration.

In recent years, quantum-mechanical approaches by first principle calculations have been increasingly used to quantify the effect of hydrogen on decohesion [31,73–75]. A key factor is that hydrogen strongly prefers to stay on the surface

compared to in the bulk, which provides a driving force for decohesion and, thereby, embrittlement. Using an equilibrium thermodynamic description, Van der Ven and Ceder [73] have obtained a complete set of traction-separation curves for decohesion along Al(111) planes with a hydrogen coverage between 0 and 1 (1 representing the saturation value). The results are displayed in Fig. 8a, revealing a decrease in the cohesive energy with increasing hydrogen coverage. The critical separation, however, was found to be insensitive to hydrogen throughout the given range.

Jiang and Carter [74] have calculated the ideal cleavage energy (equal to twice the surface energy, γ) of Fe and Al in the presence of various amounts of hydrogen within the framework of a Born-Haber thermodynamic cycle, valid for a system in equilibrium conditions. The main idea is that hydrogen dissolved in metals quickly segregate to the incipient crack surfaces as a crack begins to form. An almost linear decrease in cleavage energy with increasing hydrogen coverage is observed for both Al(111) and Fe(110), as displayed in Fig. 8b. A fit to the data for the H/Fe system yields [15]

$$\frac{\gamma(\theta_H)}{\gamma(0)} = 1 - 1.0467\theta_H + 0.1687\theta_H^2 \tag{19}$$

where θ_H is the surface hydrogen coverage, $\gamma(\theta_H)$ is the hydrogen dependent surface energy and $\gamma(0)$ is the surface energy with no hydrogen influence. The data fit is illustrated by the red line in Fig. 8b.

The definition of hydrogen coverage follows the Langmuir-McLean isotherm [76], relating it to the bulk hydrogen concentration C (unit mol H/mol Fe) through

$$\theta_H = \frac{C}{C + \exp(-\Delta G_b^0/RT)} \tag{20}$$

where ΔG_b^0 is the Gibbs energy difference between the adsorbed and bulk standard states. The hydrogen coverage as a function of hydrogen concentration is plotted in Fig. 9 for various levels of Gibbs energy ranging between 10 kJ/mol and 60 kJ/mol. It is evident that a given value of Gibbs energy covers a concentration range of about 4 orders of magnitude, where the lower bound represents a hydrogen concentration threshold for embrittlement and the upper bound represents a corresponding saturation level.

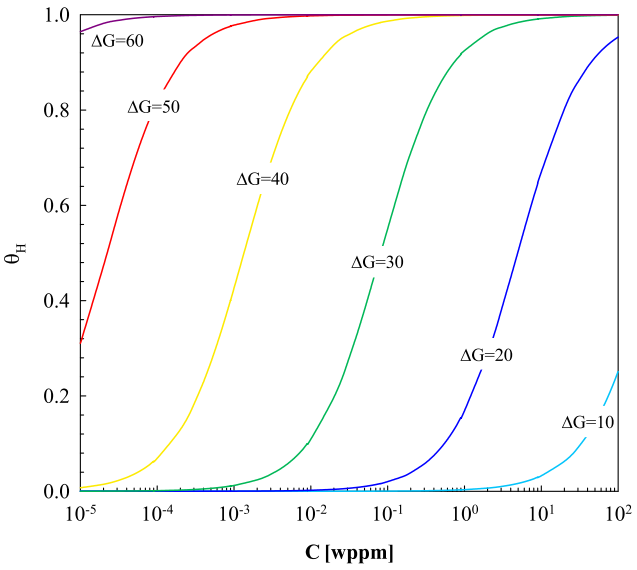

Fig. 9 – Hydrogen coverage as a function of hydrogen concentration, for various levels of Gibbs energy (kJ/mol). Plotted according to the Langmuir-McLean isotherm [76].

Extrapolation of nanometre scale quantum mechanical calculations to macroscopic scale continuum models entails some difficulty. Atomistic predictions of peak stresses are on the order of the theoretical strength of the crystal, while opening displacements are only a few angstroms [15,77,78]. Further, the cohesive zone sizes attendant to first principle calculations are on the nanometre scale, making finite element calculations unfeasible, as the mesh must fully resolve the cohesive zone in order to obtain a converged solution. Using a renormalization procedure described by Nguyen and Ortiz [77] and Hayes et al. [78] to scale the atomic-level cohesive properties up to the continuum scale, Serebrinsky et al. [15] have developed a cohesive model of fracture,

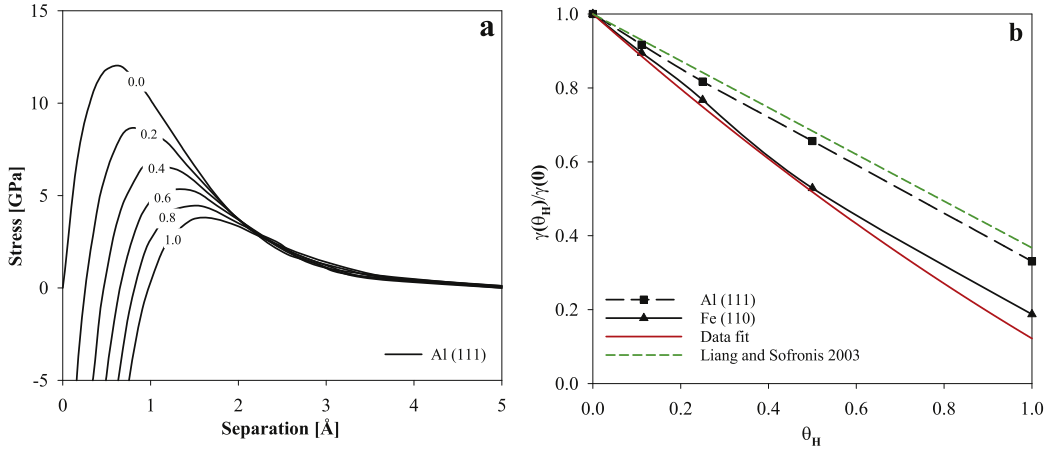

Fig. 8 – Hydrogen effect on decohesion by quantum-mechanical approaches: (a) Traction separation curves for decohesion along Al(111) planes with a hydrogen coverage between 0 and 1, by Van der Ven and Ceder [73]. (b) Cleavage energy for decohesion along Al(111) and Fe(110) as a function of hydrogen coverage, by Jiang and Carter [74].

accounting for the effect of hydrogen segregation by a quantum-mechanical treatment. Based on the relation in Equation (19), the following coupling between hydrogen coverage and the critical hydrogen dependent cohesive stress $\sigma_C(\theta_H)$ is suggested for bcc iron [15]

$$\frac{\sigma_C(\theta_H)}{\sigma_C(0)} = 1 - 1.0467\theta_H + 0.1687\theta_H^2 \quad (21)$$

The critical separation δ_C is deemed constant, insensitive to the hydrogen coverage, based on the results from Van der Ven and Ceder [73] in Fig. 8a. The influence of hydrogen, in terms of hydrogen coverage, on the cohesive strength and consequently on the cohesive energy is illustrated in Fig. 10a for the polynomial cohesive law by Needleman [60]. Using the coupling between hydrogen coverage and bulk concentration as supplied by the Langmuir-McLean isotherm, Serebrinsky et al. [15] suggested $\Delta G_b^0 = 30$ kJ/mol, which represents the trapping energy of hydrogen at a Fe grain boundary, yielding a threshold concentration of about 0.0005 wppm and an embrittlement saturation level of about 5 wppm. Hence, a concentration level close to the theoretical solubility of hydrogen in iron (about 10^{-4} wppm [40]) should not induce any significant effect on the cohesive properties, implying the importance of trapped hydrogen.

Raykar et al. [70] have proposed a hydrogen damaging effect both on the cohesive strength and on the critical separation, basing this choice on the experimentally observed reduction in both ultimate tensile strength and percentage elongation in the presence of hydrogen. A linear dependence on hydrogen concentration according to Equation (18) was chosen for both parameters. The same approach has also been applied by Gobbi et al. [79], however here with a hydrogen dependence according to the work by Serebrinsky et al. [15]. Fig. 10b illustrates hydrogen influence, in terms of hydrogen coverage, according to Equation (21), on both the cohesive strength and on the critical separation, for the polynomial cohesive law by Needleman [60]. A comparison of the effect of single and double hydrogen influence on the critical cohesive energy at fracture is made in Fig. 11, where the cohesive energy is plotted as a function of the hydrogen coverage for the two cases in Fig. 10, displaying an enhanced hydrogen damaging effect with double hydrogen influence. Although this approach displayed a reasonable fit with experimental data [70,79], no quantification of any effect of hydrogen on the critical separation is found to date.

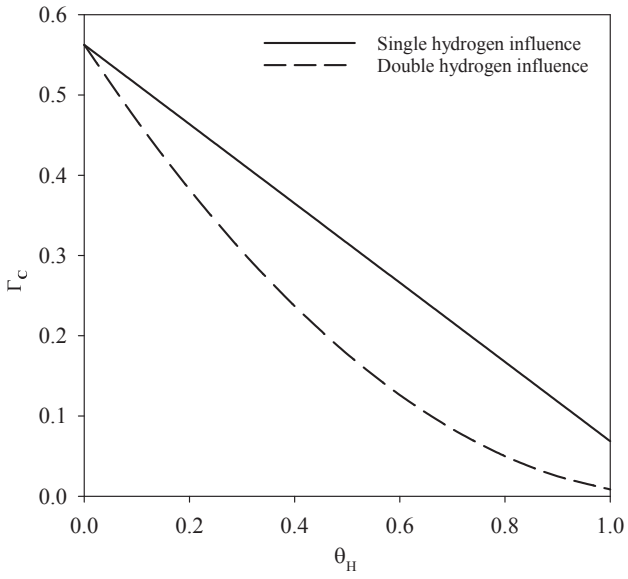

Fig. 11 – Relationship between critical cohesive energy at fracture and hydrogen coverage for the polynomial cohesive law by Needleman [60]. Single hydrogen influence denotes hydrogen reduction of the critical cohesive stress. Double hydrogen influence denotes hydrogen reduction of the critical cohesive stress and of the critical separation.

Liang and Sofronis [14] have proposed an alternative model for hydrogen decohesion, based on work by Hirth, Rice and Wang [80–82], who estimated the effect of segregated

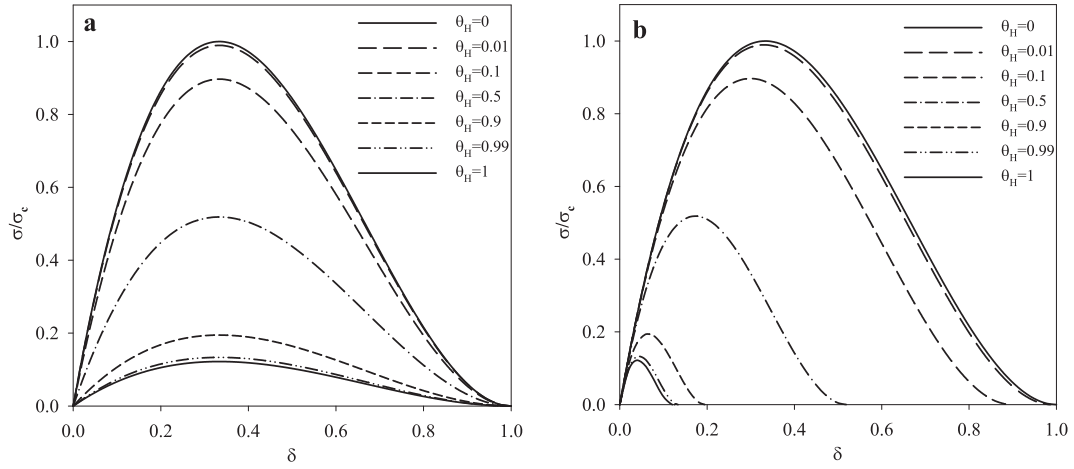

Fig. 10 – Reduction in cohesive energy at different levels of hydrogen coverage for the polynomial cohesive law by Needleman [60], where (a) illustrates hydrogen influence on the cohesive strength only (single) and (b) illustrates hydrogen influence on both the cohesive strength and the critical separation (double).

hydrogen on interface cohesion from a general thermodynamic framework. The resulting hydrogen dependent cohesive strength is expressed for two limiting cases of interfacial separation: separation at constant hydrogen concentration (denoted fast separation) given by Equation (22), and separation at constant hydrogen chemical potential (denoted slow separation) given by Equation (23)

$$\sigma_C(\Gamma) = \sigma_C(0)\left(1 - \frac{\Gamma_{max}\left(\Delta g_i^0 - \Delta g_s^0\right)}{(2\gamma_{int})_0}\frac{\Gamma}{\Gamma_{max}}\right) \quad (22)$$

$$\sigma_C(\mu) = \sigma_C(0)\left(1 - \frac{RT\Gamma_{max}}{(2\gamma_{int})_0}\ln\left(\frac{1+(m-1)(\Gamma_0/\Gamma_{max})^2}{1-(\Gamma_0/\Gamma_{max})}\right)\right) \quad (23)$$

Δg_i^0 and Δg_s^0 are the Gibbs energy of segregation for the interface and free surface, respectively, Γ/Γ_{max} is the interfacial hydrogen coverage and $m = \exp((\Delta g_i^0 - \Delta g_s^0)/RT)$. The proposed model was used to simulate separation along a chromium carbide/fcc matrix (nickel alloy 690) interface. The resulting range of polynomial cohesive laws (Needleman [60]) for various interfacial hydrogen coverage values is presented in Fig. 12. Taking parameters representative of Fe interface decohesion; $(2\gamma_{int})_0 = 3.12$ J/m^2 [82], $\Gamma_{max} = 2.65\cdot10^{-5}$ mol/m^2 [83], assuming $\Delta g_i^0 - \Delta g_s^0 = 74.5$ kJ/mol [17], the hydrogen dependent cohesive stress for the fast separation case can be estimated. The result is plotted as the green dashed line in Fig. 8b, representing a discrepancy with the results from Jiang and Carter [74] on Fe(110). It appears the data from Jiang and Carter, calculated within the framework of a Born-Haber thermodynamic cycle, overestimates the decohesion due to mobile hydrogen.

Coupling of diffusion and mechanical models

The Langmuir-McLean isotherm defines the necessary coupling between the hydrogen diffusion model in Section Hydrogen diffusion and the hydrogen-dependent cohesive law described in the previous section. The coupling takes place in two ways: first, hydrogen accelerates material damage by building up over the cohesive zone, as indicated by Equations (20) and (21). Second, hydrogen transport is influenced by the local hydrostatic stress and plastic strain fields, according to Equation (14).

Experimental results investigating the effect of hydrogen on fracture generally displays a weaker effect of hydrogen with increasing concentration [4,6,17]. Thomas et al. [4] found that the threshold stress intensity factor for hydrogen embrittlement in AERMET 100 steel decreased sharply with an increasing diffusible hydrogen concentration up to 2 wppm, and more modestly with higher concentrations. The result is displayed in Fig. 13 for a normalized threshold stress intensity factor, together with the normalized hydrogen dependent cohesive stress according to the linear model in Equation (18) and the model by Serebrinsky et al. [15], with the hydrogen concentration calculated according to the Langmuir-McLean isotherm for $\Delta G_b^0 = 30$ kJ/mol. The model by Serebrinsky et al. [15] captures the exponential embrittlement effect of hydrogen, attaining a saturation level at high concentrations. The linear model, fitted to the initial part of the experimental data, gives a reasonable approximation at low concentrations only. The results confirms the necessity of a saturating hydrogen embrittlement law, as also pointed out by Serebrinsky et al. [15].

One of the main challenges concerning the use of the Langmuir-McLean isotherm lies in its capability of capturing hydrogen embrittlement at high and low concentrations, i.e. outside the given range. Zakroczymski et al. [6] found that the main embrittlement effect occurred at a hydrogen concentration of about 26 wppm for a duplex stainless steel, while, on the contrary, Novak et al. found the fracture strength to decrease sharply up to an initial diffusible hydrogen

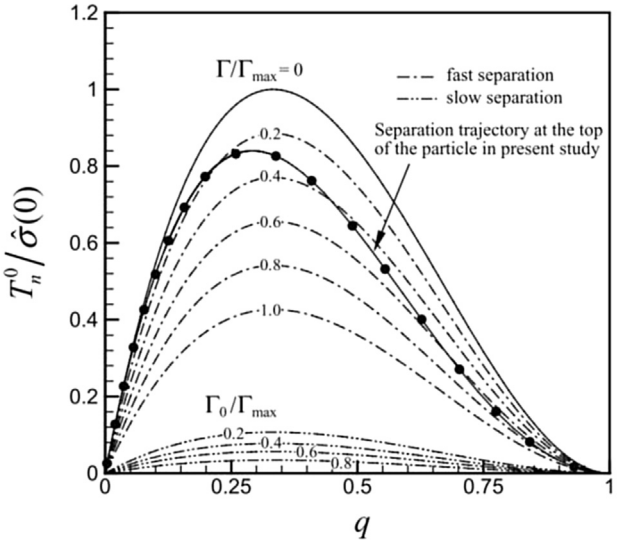

Fig. 12 – Hydrogen influenced cohesive laws from the decohesion model by Liang and Sofronis [14], T_n^0 is the normal traction and q is a non-dimensional separation parameter.

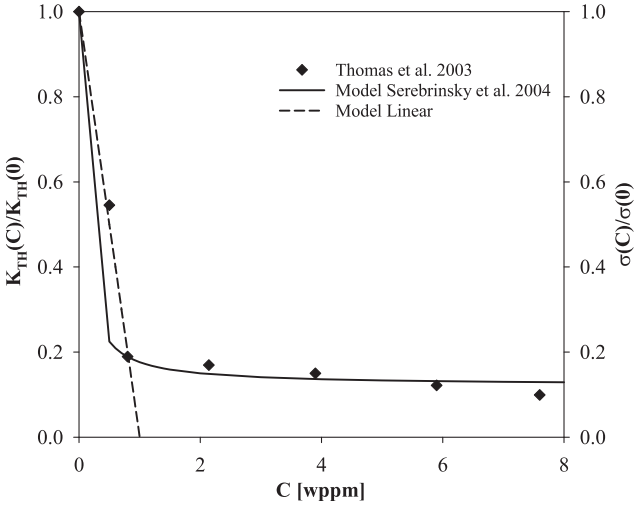

Fig. 13 – Normalized threshold stress intensity factor and normalized hydrogen dependent cohesive stress as a function of hydrogen concentration, according to experimental data by Thomas et al. [4], the linear decohesion model and the exponential decohesion model by Serebrinsky et al. [15], with $\Delta G_b^0 = 30$ kJ/mol.

concentration of only about 0.005 wppm for a high strength steel. Choosing a ΔG_b^0 level in the lower range may be justified, conforming to the findings by Novak et al. [17] and Ayas et al. [48] that the only possible trap sites associated with hydrogen embrittlement are low-binding energy traps. This would improve agreement in the high-concentration range, as can be seen from Fig. 9. Serebrinsky et al. [15] suggested that agreement for high hydrogen concentrations might be improved by considering different adsorption sites at the cracking interface, with a distribution of adsorption energies. Due to their structural complexity, internal boundaries are expected to exhibit multiple hydrogen binding energies [84]. The number of such energies should be small for phase boundaries with well-defined orientational relationship, whereas more complicated for less regular interfaces.

In Fig. 14, the resulting concentrations in Fig. 6 are replotted in terms of hydrogen coverage, calculated from Equations (20) and (21), with $\Delta G_b^0 = 30$ kJ/mol. The most striking result is that for an initial concentration of 0.00034 wppm, lattice hydrogen has a negligible effect on decohesion, reducing the critical cohesive strength with only about 0.9% at the location of maximum hydrostatic stress. For an initial concentration of 1 wppm, however, the critical cohesive strength is reduced by 82% at the notch tip and 85% at the point of maximum hydrostatic stress, thus giving only a minor variance throughout the material.

Most known attempts of capturing hydrogen embrittlement by cohesive simulations take into account two groups of hydrogen: lattice hydrogen and hydrogen trapped by dislocations. In estimating the coverage, however, there is no consensus as to whether it is a function of the lattice concentration only, the trapped concentration only, or the sum of both. While Brocks et al. [18] have used the first approach, Sofronis et al. [14,17] have applied a variation of the middle approach. Olden et al. [16,19] and Moriconi et al. [20] have applied the latter approach. Given that the model takes neither the kinetics of trapping/detrapping nor the transport of hydrogen to the surface into account, all approaches may

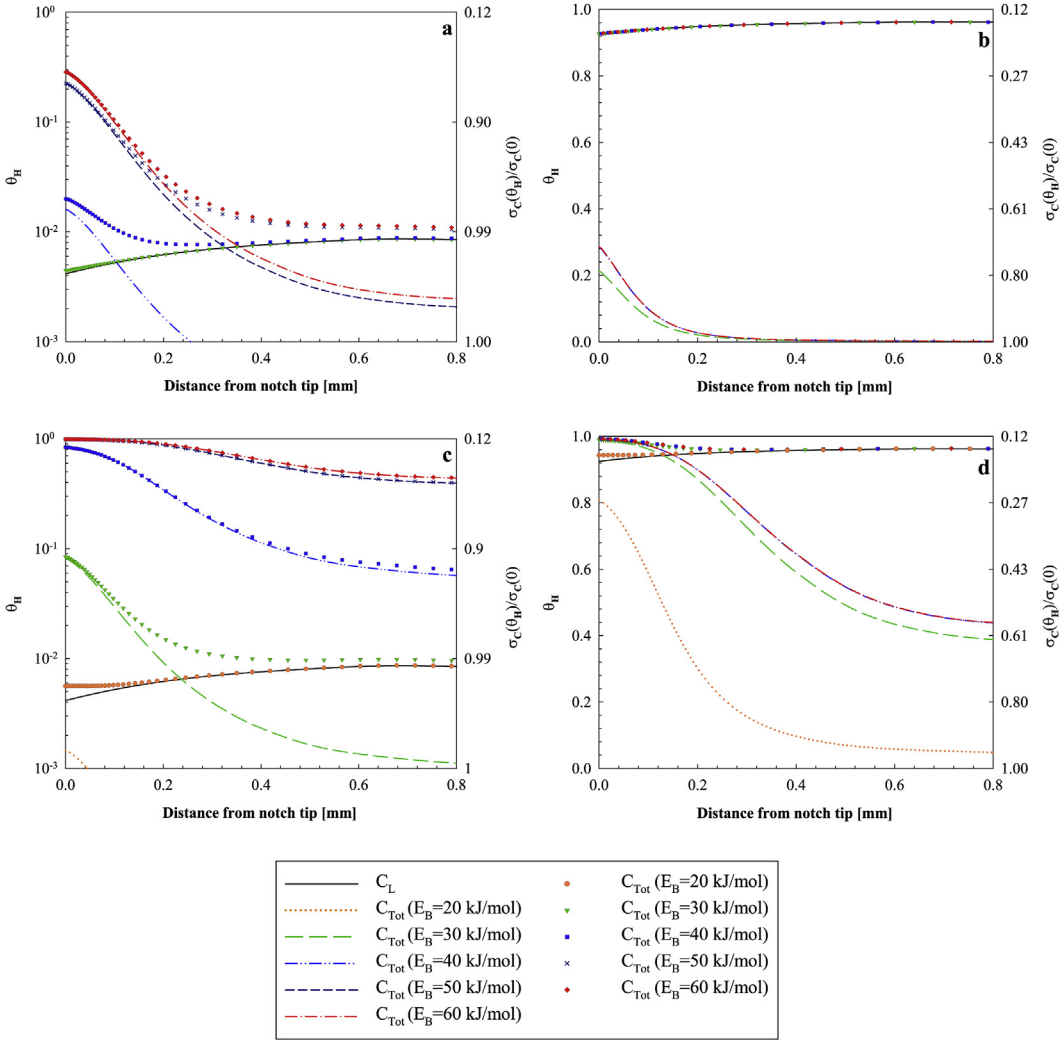

Fig. 14 – Hydrogen coverage and reduction in cohesive strength as a function of distance from the notch tip, plotted at the end of loading. $\Delta G_b^0 = 30$ kJ/mol. (a) Low trap density model, $C_0 = 0.00034$ wppm, $E_B = 30$ (C_{Tot}), 40–60 kJ/mol. (b) Low trap density model, $C_0 = 1$ wppm, $E_B = 30$–40, 60 kJ/mol. (c) High trap density model, $C_0 = 0.00034$ wppm, $E_B = 20$–60 kJ/mol. (d) High trap density model, $C_0 = 1$ wppm, $E_B = 20$–40, 60 kJ/mol.

be argued for. From Fig. 14 it is evident that the choice will have great impact on the final result. Using Fig. 14c as an example, for a trap binding energy of 60 kJ/mol, the lattice hydrogen concentration gives a reduction in critical cohesive strength of 0.9% while the trapped and the total concentration gives a reduction of 87.2%.

For the low trap density model, the maximum attainable trapped concentration of 0.033 wppm corresponds to a hydrogen coverage of 0.29 and a reduction in cohesive strength of 29%. For the high trap model, with a maximum attainable trapped concentration of 10.1 wppm, the maximum hydrogen coverage and corresponding reduction in cohesive strength are 0.99 and 87.2%, respectively. Conforming to the findings that only low binding energy traps should be considered associated with hydrogen embrittlement, putting the limit at 30 kJ/mol by realising that a hydrogen atom trapped at $E_B \geq 30$ kJ/mol will not necessarily spontaneously segregate to a grain boundary with $E_B = 30$ kJ/mol, the trapped concentration may significantly impact the critical cohesive strength only for the case of high initial hydrogen concentration (1 wppm).

Practical applications of the coupled continuum model

The capability of the model to trustfully predict hydrogen induced crack nucleation and propagation in structural steel applications is of key importance for further developments. An engineering tool, able to partly replace time consuming and costly experimental programs, should be of general validity and provide robustness and transferability to other material systems and environments. While most studies are able to reproduce single experimental results by appropriate fitting to the cohesive parameters, there still appears to be limitations on transferring these results to other hydrogen systems [19,20]. Moriconi et al. [20] have developed a cohesive model based on coupled effects between mechanical cyclic loading and hydrogen diffusion. Simulated fatigue crack growth was compared with experimental measurements on martensitic stainless steel under gaseous hydrogen. The results indicate that while the model was able to reasonably predict the fatigue crack growth behaviour under low hydrogen pressure, it failed to account for the enhanced crack growth observed at high pressures. Limitations in the model, particular in the case of lattice diffusion, were pointed out as possible explanations, however no conclusion were drawn.

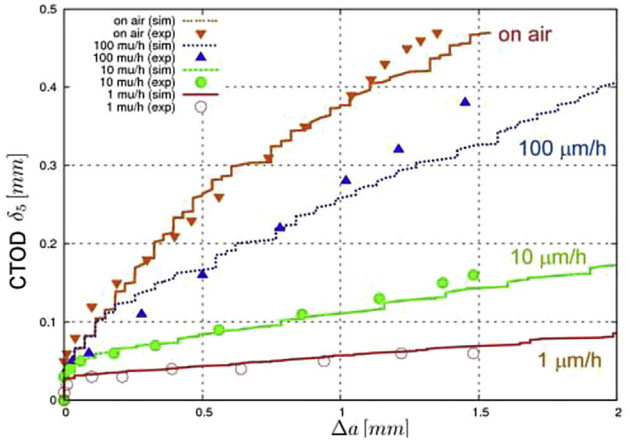

Fig. 15 – CTOD-R curves for various deformation rates, comparing experimental tests (symbol) and simulation results (lines), taken from Brocks et al. [18].

Recently, Dadfarnia et al. [34] have extended the hydrogen transport model by Sofronis and McMeeking [12] and Krom et al. [13] (Equation (15)) to account for hydrogen transport by dislocations. Moving dislocations represent moving traps that carry hydrogen atoms. Thus, hydrogen is transported by both diffusion through NILS and by mobile dislocations. Results from numerical simulations indicate that dislocation transport can contribute to an elevation of the local hydrogen concentration above levels predicted by the classical diffusion model, with the effect being larger for materials with lower hydrogen diffusion coefficient and higher dislocation trap binding energy.

Brocks et al. [18,85] have developed a model of hydrogen induced cracking, which in addition to the coupled interactions of hydrogen diffusion and reduced cohesive strength, also includes the effect of surface kinetics on hydrogen absorption and hydrogen induced softening of the local yield strength (HELP mechanism). A thorough description of the model can be found in Refs. [18,85]. By including both local hydrogen softening and hydrogen induced lowering of the local cohesive strength, the model describes an attempt in the direction of including both the HEDE and the HELP degradation mechanisms and their interactions. Simulated CTOD-R curves were compared with experimental results on high strength low alloy structural steel, with appropriate fitting of the cohesive parameters and their dependence on the lattice hydrogen concentration. The results are displayed in Fig. 15 for various deformation rates, where the two mid curves (10 µm h^{-1} and 100 µm h^{-1}) represent real predictions, capturing the rate dependence of the R-curves due to hydrogen diffusion quite well. While numerous experimental measurements are necessary in order to determine the required input parameters, the authors argue the model may, to some extent, replace expensive laboratory testing, especially considering its transferability to other systems by identifying the required parameters.

Conclusion

A coupled mass transport and cohesive zone modelling approach for simulating hydrogen induced cracking is described and discussed. Based on calculations, the main findings are summarized as follows:

- The choice of input trap binding energy and trap density formulation have significant impact on the resulting lattice, trapped and total hydrogen distributions, and on the corresponding hydrogen induced reduction of the cohesive strength.
- The use of the Langmuir-McLean isotherm as the necessary coupling between the hydrogen transport model and the hydrogen dependent cohesive law induces a hydrogen

concentration threshold level and corresponding saturation level for embrittlement, covering a concentration range of about 4 order of magnitude, dependent on the choice of ΔG_b^0. These levels have again significant influence on hydrogen induced reduction of the cohesive strength.

- To date, there is no consensus as to whether the hydrogen influence on the cohesive energy is a function of the lattice concentration only, the trapped concentration only, or the sum of both. The choice, however, will have great impact on the resulting reduction in cohesive strength, varying from 0.9% for lattice hydrogen concentration to 87.2% for trapped and total hydrogen concentration, for a given choice of input parameters.

So far, cohesive zone modelling approaches have been proved to be able to reproduce single experimental results by appropriate fitting of the cohesive parameters, however there appears to be limitations in transferring these results to other hydrogen systems. New developments within modelling of mass transport may improve the agreement. Further, transferability may be improved by appropriately identifying the required input parameters for the particular system under study.

Acknowledgements

The present work was financed by the Research Council of Norway (Petromaks 2 programme, Contract No. 234110/E30), Statoil, Gassco, Technip, POSCO and EDF Induction and performed within the frames of the ROP project (www.sintef.no/rop). The authors gratefully acknowledge the valuable input from Antonio Alvaro, Philippe Mainçon and Vidar Osen.

REFERENCES

[1] Johnson WH. On some remarkable changes produced in iron and steel by the action of hydrogen and acids. Proc R Soc Lond 1874;23:168–79.
[2] Kumnick A, Johnson H. Deep trapping states for hydrogen in deformed iron. Acta Metall 1980;28(1):33–9. http://dx.doi.org/10.1016/0001-6160(80)90038-3.
[3] Choo WY, Lee J. Thermal analysis of trapped hydrogen in pure iron. Metall Trans A 1982;13(1):135–40. http://dx.doi.org/10.1007/BF02642424.
[4] Thomas RLS, Scully JR, Gangloff RP. Internal hydrogen embrittlement of ultrahigh-strength AERMET 100 steel. Metall Mater Trans A 2003;34(2):327–44. http://dx.doi.org/10.1007/s11661-003-0334-3.
[5] Li D, Gangloff RP, Scully JR. Hydrogen trap states in ultrahigh-strength AERMET 100 steel. Metall Mater Trans A 2004;35(3):849–64. http://dx.doi.org/10.1007/s11661-004-0011-1.
[6] Zakroczymski T, Glowacka A, Swiatnicki W. Effect of hydrogen concentration on the embrittlement of a duplex stainless steel. Corros Sci 2005;47(6):1403–14. http://dx.doi.org/10.1016/j.corsci.2004.07.036.
[7] Hardie D, Charles EA, Lopez AH. Hydrogen embrittlement of high strength pipeline steels. Corros Sci 2006;48(12):4378–85. http://dx.doi.org/10.1016/j.corsci.2006.02.011.
[8] Moro I, Briottet L, Lemoine P, Andrieu E, Blanc C, Odemer G. Hydrogen embrittlement susceptibility of a high strength steel X80. Mater Sci Eng A 2010;527(27):7252–60. http://dx.doi.org/10.1016/j.msea.2010.07.027.
[9] Alvaro A, Olden V, Macadre A, Akselsen OM. Hydrogen embrittlement susceptibility of a weld simulated X70 heat affected zone under H2 pressure. Mater Sci Eng A 2014;597:29–36. http://dx.doi.org/10.1016/j.msea.2013.12.042.
[10] Kheradmand N, Johnsen R, Olsen JS, Barnoush A. Effect of hydrogen on the hardness of different phases in super duplex stainless steel. Int J Hydrogen Energy 2016;41(1):704–12. http://dx.doi.org/10.1016/j.ijhydene.2015.10.106.
[11] Hajilou T, Deng Y, Rogne BR, Kheradmand N, Barnoush A. In situ electrochemical microcantilever bending test: a new insight into hydrogen enhanced cracking. Scr Mater 2017;132:17–21. http://dx.doi.org/10.1016/j.scriptamat.2017.01.019.
[12] Sofronis P, McMeeking R. Numerical analysis of hydrogen transport near a blunting crack tip. J Mech Phys Solids 1989;37(3):317–50. http://dx.doi.org/10.1016/0022-5096(89)90002-1.
[13] Krom A, Koers R, Bakker A. Hydrogen transport near a blunting crack tip. J Mech Phys Solids 1999;47(4):971–92. http://dx.doi.org/10.1016/S0022-5096(98)00064-7.
[14] Liang Y, Sofronis P. Toward a phenomenological description of hydrogen-induced decohesion at particle/matrix interfaces. J Mech Phys Solids 2003;51(8):1509–31. http://dx.doi.org/10.1016/S0022-5096(03)00052-8.
[15] Serebrinsky A, Carter EA, Ortiz M. A quantum-mechanically informed continuum model of hydrogen embrittlement. J Mech Phys Solids 2004;52:2403–30. http://dx.doi.org/10.1016/j.jmps.2004.02.010.
[16] Olden V, Thaulow C, Johnsen R, Østby E, Berstad T. Influence of hydrogen from cathodic protection on the fracture susceptibility of 25%Cr duplex stainless steel-constant load SENT testing and FE-modelling using hydrogen influenced cohesive zone elements. Eng Fract Mech 2009;76(7):827–44. http://dx.doi.org/10.1016/j.engfracmech.2008.11.011.
[17] Novak P, Yuan R, Somerday BP, Sofronis P, Ritchie RO. A statistical, physical-based, micro-mechanical model of hydrogen-induced intergranular fracture in steel. J Mech Phys Solids 2010;58(2):206–26. http://dx.doi.org/10.1016/j.jmps.2009.10.005.
[18] Brocks W, Falkenberg R, Scheider I. Coupling aspects in the simulation of hydrogen-induced stress-corrosion cracking. Proc IUTAM 2012;3:11–24. http://dx.doi.org/10.1016/j.piutam.2012.03.002.
[19] Alvaro A, Olden V, Akselsen OM. 3D cohesive modelling of hydrogen embrittlement in the heat affected zone of an X70 pipeline steel - Part II. Int J Hydrogen Energy 2014;39:3528–41. http://dx.doi.org/10.1016/j.ijhydene.2013.12.097.
[20] Moriconi C, Hénaff G, Halm D. Cohesive zone modeling of fatigue crack propagation assisted by gaseous hydrogen in metals. Int J Fatigue 2014;68:56–66. http://dx.doi.org/10.1016/j.ijfatigue.2014.06.007.
[21] Troiano AR. The role of hydrogen and other interstitials in the mechanical behaviour of metals. Trans ASM 1960;52:54–80.
[22] Oriani RA. The diffusion and trapping of hydrogen in steel. Acta Metall 1970;18(1):147–57. http://dx.doi.org/10.1016/0001-6160(70)90078-7.
[23] Oriani RA. A mechanistic theory of hydrogen embrittlement of steels. Berichte Bunsenges für Phys Chem 1972;76(8):848–57. http://dx.doi.org/10.1002/bbpc.19720760864.
[24] Oriani RA, Josephic PH. Equilibrium and kinetic studies of the hydrogen-assisted cracking of steel. Acta Metall

1977;25(9):979–88. http://dx.doi.org/10.1016/0001-6160(77)90126-2.
[25] Gerberich WW, Marsh PG, Hoehn JW. Hydrogen induced cracking mechanisms - are there critical experiments?. In: Hydrog. Eff. Mater. Minerals, Metals & Materials Society (TMS); 1996. p. 539–51. http://dx.doi.org/10.1002/9781118803363.ch47.
[26] Birnbaum H, Sofronis P. Hydrogen-enhanced localized plasticity-a mechanism for hydrogen-related fracture. Mater Sci Eng A 1994;176(1–2):191–202. http://dx.doi.org/10.1016/0921-5093(94)90975-X.
[27] Sofronis P, Liang Y, Aravas N. Hydrogen induced shear localization of the plastic flow in metals and alloys. Eur J Mech A - Solids 2001;20:857–72. http://dx.doi.org/10.1016/S0997-7538(01)01179-2.
[28] Delafosse D, Magnin T. Hydrogen induced plasticity in stress corrosion cracking of engineering systems. Eng Fract Mech 2001;68(6):693–729. http://dx.doi.org/10.1016/S0013-7944(00)00121-1.
[29] Liang Y, Sofronis P, Aravas N. On the effect of hydrogen on plastic instabilities in metals. Acta Mater 2003;51(9):2717–30. http://dx.doi.org/10.1016/S1359-6454(03)00081-8.
[30] Robertson IM, Birnbaum HK, Sofronis P. Chapter 91 Hydrogen effects on plasticity. Dislocations Solids 2009;15(09):249–93. http://dx.doi.org/10.1016/S1572-4859(09)01504-6.
[31] Alvaro A, Thue Jensen I, Kheradmand N, Løvvik OM, Olden V. Hydrogen embrittlement in nickel, visited by first principles modeling, cohesive zone simulation and nanomechanical testing. Int J Hydrogen Energy 2015;40(47):16892–900. http://dx.doi.org/10.1016/j.ijhydene.2015.06.069.
[32] Yu H, Olsen JS, Alvaro A, Olden V, He J, Zhang Z. A uniform hydrogen degradation law for high strength steels. Eng Fract Mech 2016;157:56–71. http://dx.doi.org/10.1016/j.engfracmech.2016.02.001.
[33] Dadfarnia M, Sofronis P, Neeraj T. Hydrogen interaction with multiple traps: can it be used to mitigate embrittlement? Int J Hydrogen Energy 2011;36(16):10141–8. http://dx.doi.org/10.1016/j.ijhydene.2011.05.027.
[34] Dadfarnia M, Martin ML, Nagao A, Sofronis P, Robertson IM. Modeling hydrogen transport by dislocations. J Mech Phys Solids 2015;78:511–25. http://dx.doi.org/10.1016/j.jmps.2015.03.002.
[35] Martínez-Pañeda E, del Busto S, Niordson CF, Betegón C. Strain gradient plasticity modeling of hydrogen diffusion to the crack tip. Int J Hydrogen Energy 2016;41(24):10265–74. http://dx.doi.org/10.1016/j.ijhydene.2016.05.014.
[36] Turnbull A, Hutchings RB, Ferriss DH. Modelling of thermal desorption of hydrogen from metals. Mater Sci Eng A 1997;238:317–28. http://dx.doi.org/10.1016/S0921-5093(97)00426-7.
[37] Pressouyre GM, Bernstein IM. A quantitative analysis of hydrogen trapping. Metall Trans A 1978;9(11):1571–80. http://dx.doi.org/10.1007/BF02661939.
[38] Thomas GJ. Hydrogen trapping in FCC metals. In: Bernstein IM, Thompson AW, editors. Hydrog. Eff. Mater. Transactions of the Metallurgical Society of AIME; 1980. p. 77–85.
[39] Yagodzinskyy Y, Ivanchenko M, Hänninen H. Hydrogen-dislocation interaction in austenitic stainless steel studied with mechanical loss spectroscopy. Solid State Phenom 2012;184:227–32. http://dx.doi.org/10.4028/www.scientific.net/SSP.184.227.
[40] Hirth JP. Effects of hydrogen on the properties of iron and steel. Metall Trans A 1980;11(6):861–90. http://dx.doi.org/10.1007/BF02654700.
[41] Paes de Oliveira C, Aucouturier M, Lacombe P. Hydrogen trapping in BCC Fe-Cr Alloy as studied by microautoradiography - contribution of carbon-hydrogen interaction - consequences on hydrogen cracking. Corrosion 1980;36(2):53–9. http://dx.doi.org/10.5006/0010-9312-36.2.53.
[42] Turnbull A, Hutchings RB. Analysis of hydrogen atom transport in a two-phase alloy. Mater Sci Eng A 1994;177(1–2):161–71. http://dx.doi.org/10.1016/0921-5093(94)90488-X.
[43] Olden V, Thaulow C, Johnsen R. Modelling of hydrogen diffusion and hydrogen induced cracking in supermartensitic and duplex stainless steels. Mater Des 2008;29(10):1934–48. http://dx.doi.org/10.1016/j.matdes.2008.04.026.
[44] McNabb A, Foster PK. A new analysis of the diffusion of hydrogen in iron and ferritic steels. Trans Metall Soc AIME 1963;227:618–27.
[45] San Marchi C, Somerday BP, Robinson SL. Permeability, solubility and diffusivity of hydrogen isotopes in stainless steels at high gas pressure. Int J Hydrogen Energy 2007;32(1):100–16. http://dx.doi.org/10.1016/j.ijhydene.2006.05.008.
[46] Lufrano J, Sofronis P, Symons D. Hydrogen transport and large strain elastoplasticity near a notch in alloy X-750. Eng Fract Mech 1998;59(6):827–45. http://dx.doi.org/10.1016/S0013-7944(97)00142-2.
[47] Alvaro A, Olden V, Akselsen OM. 3D cohesive modelling of hydrogen embrittlement in the heat affected zone of an X70 pipeline steel. Int J Hydrogen Energy 2013;38(18):7539–49. http://dx.doi.org/10.1016/j.ijhydene.2013.02.146.
[48] Ayas C, Deshpande VS, Fleck NA. A fracture criterion for the notch strength of high strength steels in the presence of hydrogen. J Mech Phys Solids 2014;63:80–93. http://dx.doi.org/10.1016/j.jmps.2013.10.002.
[49] Mehrer H. Diffusion in solids. 1st ed. Springer-Verlag Berlin Heidelberg; 2007. http://dx.doi.org/10.1007/978-3-540-71488-0.
[50] Porter DA, Easterling KE, Sherif MY. Phase transformations in metals and alloys. 3rd ed. Taylor and Francis Group: CRC Press; 2009.
[51] Crank J. The mathematics of diffusion. 2nd ed. Oxford University Press; 1975.
[52] Grong O. Metallurgical modelling of welding. 2nd ed. The Institute of Materials; 1997.
[53] Chateau JP, Delafosse D, Magnin T. Numerical simulations of hydrogen-dislocation interactions in fcc stainless steels.: part I: hydrogen-islocation interactions in bulk crystals. Acta Mater 2002;50(6):1507–22. http://dx.doi.org/10.1016/S1359-6454(02)00008-3.
[54] Chateau JP, Delafosse D, Magnin T. Numerical simulations of hydrogen–dislocation interactions in fcc stainless steels.: part II: hydrogen effects on crack tip plasticity at a stress corrosion crack. Acta Mater 2002;50(6):1523–38. http://dx.doi.org/10.1016/S1359-6454(02)00009-5.
[55] Li JCM, Oriani RA, Darken LS. The thermodynamic of stressed solids. Z für Phys Chem Neue Folge 1966;49(3–4):271–90. http://dx.doi.org/10.1524/zpch.1966.49.3_5.271.
[56] Barenblatt GI. The mathematical theory of equilibrium cracks in brittle fracture. Adv Appl Mech 1962;7:55–129. http://dx.doi.org/10.1016/S0065-2156(08)70121-2.
[57] Dugdale DS. Yielding of steel sheets containing slits. J Mech Phys Solids 1960;8:100–4. http://dx.doi.org/10.1016/0022-5096(60)90013-2.
[58] Cornec A, Scheider I, Schwalbe KH. On the practical application of the cohesive model. Eng Fract Mech 2003;70:1963–87. http://dx.doi.org/10.1016/S0013-7944(03)00134-6.
[59] Hillerborg A, Modéer M, Petersson P-E. Analysis of crack formation and crack growth in concrete by means of fracture mechanics and finite elements. Cem Concr Res 1976;6(6):773–81. http://dx.doi.org/10.1016/0008-8846(76)90007-7.

[60] Needleman A. A continuum model for void nucleation by inclusion debonding. J Appl Mech 1987;54(3):525–31. http://dx.doi.org/10.1115/1.3173064.
[61] Scheider I. Simulation of cup-cone fracture in round bars using the cohesive zone model. In: First MIT conf. comput. fluid solid mech. Elsevier; 2001. p. 460–2.
[62] Shet C, Chandra N. Analysis of energy balance when using cohesive zone models to simulate fracture processes. J Eng Mater Technol ASME 2002;124(4):440–50. http://dx.doi.org/10.1115/1.1494093.
[63] Brocks W, Cornec A, Scheider I. Numerical and computational methods. In: Milne I, Ritchie RO, Karihaloo B, editors. Compr. struct. integr. Elsevier; 2003. p. 127–209.
[64] Scheider I, Brocks W. The effect of the traction separation law on the results of cohesive zone crack propagation analyses. Key Eng Mater 2003;251–252:313–8. http://dx.doi.org/10.4028/www.scientific.net/KEM.251-252.313.
[65] Tvergaard V, Hutchinson JW. The relation between crack growth resistance and fracture process parameters in elastic-plastic solids. J Mech Phys Solids 1992;40(6):1377–97. http://dx.doi.org/10.1016/0022-5096(92)90020-3.
[66] Gao YF, Bower AF. A simple technique for avoiding convergence problems in finite element simulations of crack nucleation and growth on cohesive interfaces. Model Simul Mater Sci Eng 2004;12:453–63. http://dx.doi.org/10.1088/0965-0393/12/3/007.
[67] Yu H, Olsen JS, Olden V, Alvaro A, He J, Zhang Z. Viscous regularization for cohesive zone modeling under constant displacement: an application to hydrogen embrittlement simulation. Eng Fract Mech 2016;166:23–42. http://dx.doi.org/10.1016/j.engfracmech.2016.08.019.
[68] Olden V, Thaulow C, Johnsen R, Østby E. Cohesive zone modeling of hydrogen-induced stress cracking in 25% Cr duplex stainless steel. Scr Mater 2007;57(7):615–8. http://dx.doi.org/10.1016/j.scriptamat.2007.06.006.
[69] Scheider I, Pfuff M, Dietzel W. Simulation of hydrogen assisted stress corrosion cracking using the cohesive model. Eng Fract Mech 2008;75(15):4283–91. http://dx.doi.org/10.1016/j.engfracmech.2007.10.002.
[70] Raykar NR, Maiti SK, Singh Raman RK, Aryan S. Study of hydrogen concentration dependent growth of external annular crack in round tensile specimen using cohesive zone model. Eng Fract Mech 2013;106:49–66. http://dx.doi.org/10.1016/j.engfracmech.2013.04.007.
[71] Barrera O, Cocks A. Computational modelling of hydrogen embrittlement in welded structures. Philos Mag 2013;93(20):2680–700. http://dx.doi.org/10.1080/14786435.2013.785638.
[72] Oriani RA, Josephic PH. Equilibrium aspects of hydrogen-induced cracking of steels. Acta Metall 1974;22(9):1065–74. http://dx.doi.org/10.1016/0001-6160(74)90061-3.
[73] Van der Ven A, Ceder G. The thermodynamics of decohesion. Acta Mater 2004;52:1223–35. http://dx.doi.org/10.1016/j.actamat.2003.11.007.
[74] Jiang DE, Carter EA. First principles assessment of ideal fracture energies of materials with mobile impurities: implications for hydrogen embrittlement of metals. Acta Mater 2004;52:4801–7. http://dx.doi.org/10.1016/j.actamat.2004.06.037.
[75] Zhong L, Wu R, Freeman AJ, Olson GB. Charge transfer mechanism of hydrogen-induced intergranular embrittlement of iron. Phys Rev B 2000;62(21):13938–41. http://dx.doi.org/10.1103/PhysRevB.62.13938.
[76] Hondros ED, Seah MP. The theory of grain boundary segregation in terms of surface adsorption analogues. Metall Trans A 1977;8(9):1363–71. http://dx.doi.org/10.1007/BF02642850.
[77] Nguyen O, Ortiz M. Coarse-graining and renormalization of atomistic binding relations and universal macroscopic cohesive behavior. J Mech Phys Solids 2002;50(8):1727–41. http://dx.doi.org/10.1016/S0022-5096(01)00133-8.
[78] Hayes RL, Ortiz M, Carter EA. Universal binding-energy relation for crystals that accounts for surface relaxation. Phys Rev B 2004;69(17):172104. http://dx.doi.org/10.1103/PhysRevB.69.172104.
[79] Gobbi G, Colombo C, Miccoli S, Vergani L. A numerical model to study the hydrogen embrittlement effect. Proc Eng 2014;74:460–3. http://dx.doi.org/10.1016/j.proeng.2014.06.297.
[80] Hirth JP, Rice JR. On the thermodynamics of adsorption at interfaces as it influences decohesion. Metall Trans A 1980;11(9):1501–11. http://dx.doi.org/10.1007/BF02654514.
[81] Rice J, Wang J-S. Embrittlement of interfaces by solute segregation. Mater Sci Eng A 1989;107:23–40. http://dx.doi.org/10.1016/0921-5093(89)90372-9.
[82] Wang J-S. The thermodynamics aspects of hydrogen induced embrittlement. Eng Fract Mech 2001;68(6):647–69. http://dx.doi.org/10.1016/S0013-7944(00)00120-X.
[83] Wang J-S, Vehoff H. The effect of the mobility of segregated atoms on interfacial embrittlement. Scr Metall Mater 1991;25(6):1339–44. http://dx.doi.org/10.1016/0956-716X(91)90411-S.
[84] Myers SM, Baskes MI, Birnbaum HK, Corbett JW, DeLeo GG, Estreicher SK, et al. Hydrogen interactions with defects in crystalline solids. Rev Mod Phys 1992;64(2):559–617. http://dx.doi.org/10.1103/RevModPhys.64.559.
[85] Falkenberg R, Brocks W, Dietzel W, Scheider I. Modelling the effect of hydrogen on ductile tearing resistance of steel. Int J Mater Res 2010;101(8):989–96. http://dx.doi.org/10.3139/146.110368.